

## Spin-dependent tunneling spectroscopy for interface characterization of epitaxial Fe/MgO/Fe magnetic tunnel junctions

G. X. Du,<sup>1</sup> S. G. Wang,<sup>1,2,\*</sup>† Q. L. Ma,<sup>1</sup> Yan Wang,<sup>1</sup> R. C. C. Ward,<sup>2</sup> X.-G. Zhang,<sup>3,\*</sup>‡ C. Wang,<sup>4</sup>  
A. Kohn,<sup>4</sup> and X. F. Han<sup>1</sup>

<sup>1</sup>State Key Laboratory of Magnetism, Beijing National Laboratory for Condensed Matter Physics, Institute of Physics, Chinese Academy of Sciences, Beijing 100190, China

<sup>2</sup>Clarendon Laboratory, Department of Physics, University of Oxford, Oxford OX1 3PU, United Kingdom

<sup>3</sup>Center for Nanophase Materials Sciences and Computer Science and Mathematics Division, Oak Ridge National Laboratory, P.O. Box 2008, Oak Ridge, Tennessee 37831-6493, USA

<sup>4</sup>Department of Materials, University of Oxford, Oxford OX1 3PH, United Kingdom

(Received 13 September 2009; revised manuscript received 21 January 2010; published 26 February 2010)

Low-voltage spin-dependent tunneling spectroscopy of an epitaxial Fe/MgO/Fe magnetic tunnel junction is measured and compared to first-principles calculation of the tunneling conductance. The measured dynamic conductance ( $dI/dV$ ) in the parallel configuration shows distinct asymmetric features as a function of the bias voltage. The peaks are independent of barrier thickness, magnetic field, and temperature. With the help of the first-principles calculations, positive and negative bias spectra can be related to different types of Fe/MgO interfaces.

DOI: 10.1103/PhysRevB.81.064438

PACS number(s): 85.75.-d, 75.70.Cn

The discovery of tunneling magnetoresistance (TMR) (Refs. 1–3) and giant TMR (Refs. 4–11) in magnetic tunnel junctions (MTJs) leads to an intense interest in the spin-dependent tunneling spectroscopy.<sup>12–17</sup> By measuring the first and second derivatives of the  $I$ - $V$  curve of a tunnel junction, it is hoped that features such as interface resonant states<sup>18</sup> can be revealed. In tunneling spectroscopy, measured  $dI/dV$  curves of common tunnel junctions are rather featureless. Peaks in  $d^2I/dV^2$  are used to identify inelastic processes in tunneling, commonly called inelastic electron-tunneling (IET) spectroscopy. Few experiments have been able to produce  $dI/dV$  curve with identifiable features that can be compared to theory.

A MTJ has two states that are switched by a magnetic field. One is an antiparallel (AP) configuration where the magnetizations of two electrodes are opposite to each other and the other a parallel (P) configuration where the magnetizations are aligned. Exception for one or two works,<sup>19</sup> most  $dI/dV$  measurements for both configurations are featureless. However, the IET spectra ( $d^2I/dV^2$ ) for two configurations are very different. There are usually multiple peaks in the  $d^2I/dV^2$  of the P configuration, which are generally identified with the electron-magnon- and electron-phonon-scattering processes. For the AP configuration, the dominant features are the peaks in  $d^2I/dV^2$  due to the logarithmic singularity of the zero-bias anomaly, also attributed to the electron-magnon scattering.<sup>20</sup> Due to the lack of features in the measured dynamic conductance, spin-dependent tunneling spectroscopy has not been able to provide much information on interface structures of MTJs despite the realization that such measurements should be sensitive to the changes at the interfaces.<sup>21</sup>

In this paper, we report measurements of the dynamic conductance and IET spectrum in fully epitaxial Fe/MgO/Fe MTJs. By carefully eliminating most of the junction defects that can smear out features in the spectroscopy measurement, clear features emerge in the dynamic conductance ( $dI/dV - V$ ) of the P configuration. The peaks in  $dI/dV$  are matched to the peaks in the transmission probability calculated from

first principles under (nonself-consistent) finite biases for three types of Fe/MgO interface structure, symmetry Fe/MgO/Fe junction, asymmetric Fe/MgO/vacancy/Fe, and Fe/FeO/MgO/Fe junctions. Furthermore, features in  $d^2I/dV^2$  can be identified from the peaks in  $dI/dV$  which are accounted for from the ballistic first-principles calculations, indicating that no inelastic peaks in the so-called IET spectra are observed in our epitaxial Fe/MgO/Fe MTJs. This result provides a new understanding of the spin-dependent tunneling spectroscopy of MgO-based epitaxial MTJs.

Fully epitaxial Fe/MgO/Fe structures were grown on MgO(001) substrate by molecular-beam epitaxy. Detailed descriptions of the growth process, the structural characterization, and junction fabrication can be found elsewhere.<sup>22–24</sup> The magnetotransport properties were measured in a physical properties measurement system using a standard four-probe technique. Dynamic conductance ( $dI/dV - V$ ) and IET spectrum ( $d^2I/dV^2 - V$ ) were measured at 30.79 Hz with an ac modulation voltage of 4 mV using a standard lock-in method.<sup>9,12</sup>

Figure 1(a) shows the typical  $R$ - $H$  loops at 4.2 K for the MTJs with structure of Fe(25)/MgO( $t$ )/Fe(10)/IrMn(10) (thicknesses in nanometer), where  $t_{\text{MgO}}$  is 2.1 and 3.0 nm with TMR ratios of 218% and 318%, respectively. The resistance is normalized by value in the P configuration. The junction shows low resistance in the P configuration and high resistance in the AP configuration. The thickness and temperature dependence of the TMR ratio was published elsewhere.<sup>25</sup> Figure 1(b) presents the dynamic resistance ( $dV/dI$ ) as a function of bias voltage for junctions with  $t_{\text{MgO}}=2.1$  nm at 4.2 K in the P and AP configurations, where the constant current mode is used. The dynamic resistance in the AP configuration shows a typical bias dependence with a zero-bias anomaly and in P configuration it does not show a large variation.

In Fig. 2, the dynamic conductance ( $dI/dV$ ) is shown in panels (a) and (b) and IET spectrum ( $d^2I/dV^2 - V$ ) is shown in panels (c) and (d) for the P and AP configurations, respec-

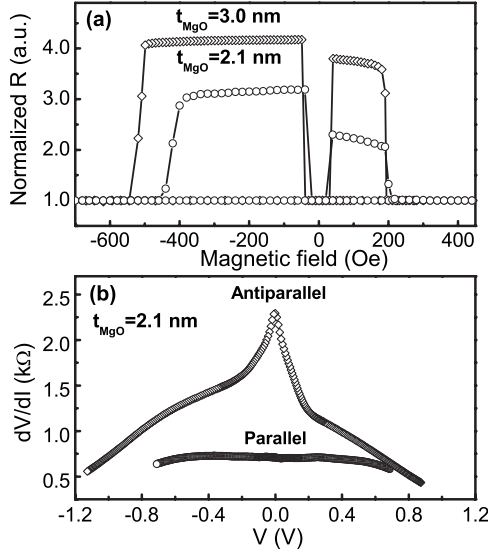


FIG. 1. (a) Normalized resistance vs magnetic fields at 4.2 K in junctions with  $t_{\text{MgO}} = 2.1$  and 3.0 nm, respectively. (b) Dynamic resistance ( $dV/dI$ ) vs bias voltage for junctions with  $t_{\text{MgO}} = 2.1$  nm.

tively. The data were taken at 4.2 K for the junction with  $t_{\text{MgO}} = 2.1$  nm. Here, the positive bias means the dc current flowing from bottom to top electrode or electrons injected from the top electrode. There is a strong asymmetry in the dynamic conductance between positive and negative biases, even though the epitaxial Fe/MgO/Fe structure is stoichiometrically symmetric. This asymmetry is further evident by a broad shoulder around 0.2 V in Fig. 2(b), which is only observed in the positive bias. Such asymmetry has been reported previously.<sup>13,19</sup> Possible explanations are the interface dislocations,<sup>13</sup> different electronic structures of the top and bottom electrodes at Fe/MgO interfaces,<sup>8</sup> and formation of Fe-O layer at the interfaces.<sup>23,26,27</sup> The  $dI/dV$  curve for the P configuration in Fig. 2(a) shows some unambiguous features. Similar but much less pronounced features were seen in a previous work<sup>19</sup> but no explanation was offered in that work.

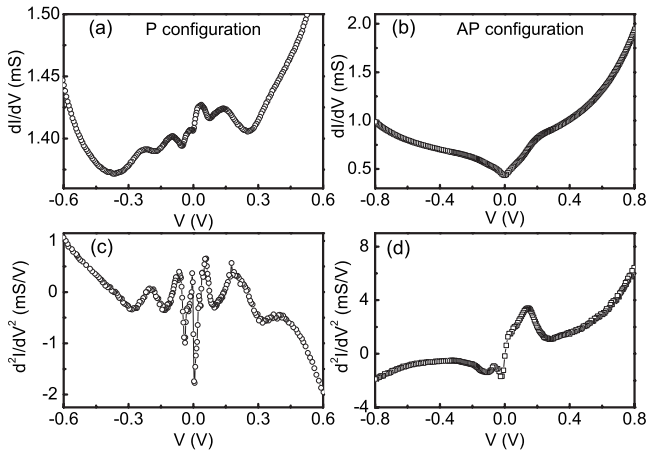


FIG. 2. [(a) and (b)] Dynamic conductance ( $dI/dV$ ) and [(c) and (d)] IET spectrum for the P and AP configurations at 4.2 K for the junction with  $t_{\text{MgO}} = 2.1$  nm.

In Fig. 2(c), the IET spectrum shows several peaks, all of which can be obtained from the derivative of the peaks in Fig. 2(a). It is necessary to point out that the IET spectrum here is measured by lock-in method, not numerically obtained from  $dI/dV$  data.<sup>14</sup>

To understand the origin of these peaks, dynamic conductance and IET spectra were measured for three samples with different barrier thicknesses (3.0, 2.1, and 1.5 nm) and as functions of the temperature and applied magnetic fields. We did not observe any difference in the peak positions between three samples. The sample independence and the barrier thickness independence exclude both the defect scattering inside the barrier and the interference effect of tunneling states in the MgO barrier<sup>4,7,13</sup> as possible origins of these peaks. In-plane magnetic fields up to 10 T (not shown here) were applied during the measurement for the P configuration (AP configuration is possible only at low magnetic fields). The peaks do not show any changes under the magnetic fields. With respect to temperature variation, all peak positions remain unchanged below 77 K. Above 77 K the peaks become unobservable due to thermal smearing. The absence of any magnetic field dependence and temperature dependence of the peak positions also make magnon and phonon scattering unlikely origins.

Next we present the first-principles calculation of the conductance as a function of bias and compare the calculation with the experimental measurements. From Fig. 2 we can see that the features in the dynamic conductance and IET spectrum are concentrated at low biases, below 0.4 V. At low bias voltages for the P configuration the effect of charge rearrangement due to the applied bias is small and the main effect is the shift of the electrostatic potential in the two electrodes by  $\pm eV/2$ .<sup>28</sup> Furthermore, over a narrow energy window  $E_F \pm eV/2$ , where  $E_F$  is the Fermi energy at zero bias, the transmission can be approximated by a linear function of the energy. This allows us to write the total current as

$$I(V) = \frac{1}{e} \int_{E_F - eV/2}^{E_F + eV/2} G(E, V) dE \approx G(E_F, V)V, \quad (1)$$

where  $G(E, V)$  is the conductance calculated at energy  $E$  and with the electrostatic potential in the two electrodes shifted by  $\pm eV/2$ , respectively. The dynamic conductance is then,

$$\frac{dI(V)}{dV} = G(E_F, V) + V \frac{\partial G(E_F, V)}{\partial V} \approx G(E_F, V). \quad (2)$$

Here neglecting the second term does not change qualitatively the peaks of the dynamic conductance. The calculation of  $G(E_F, V)$  is carried out with the first-principles layer Korringa-Kohn-Rostoker approach.<sup>29</sup>

In the previous works,<sup>4,27</sup> an ideally symmetric Fe/MgO/Fe structure and an asymmetric Fe/FeO/MgO/Fe structure where a single atomic FeO layer is assumed at the bottom interface were calculated. Here a third asymmetric structure, Fe/MgO/vacancy/Fe, with vacancies on the oxygen sublattice of the top MgO layer, is also calculated. It was pointed out by Yuasa *et al.*<sup>7</sup> that the oxygen vacancies might form due to the decomposing process of MgO into O atoms that form O<sub>2</sub> molecules in ultrahigh-vacuum chamber and the

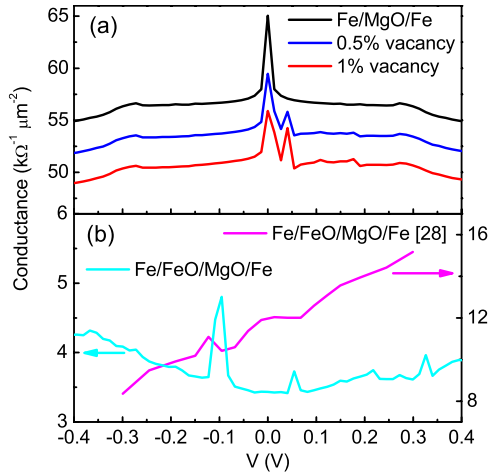


FIG. 3. (Color online) Calculated parallel conductance as a function of bias voltage for junctions (a) symmetric Fe/MgO/Fe, asymmetric Fe/MgO/0.5%vacancy/Fe, and Fe/MgO/1%vacancy/Fe, and (b) asymmetric Fe/FeO/MgO/Fe (this work and Ref. 28).

continuous pumping out of the chamber during MgO growth by evaporation. However, they found that the vacancy concentration did not exceed their measurement resolution of 1%. A previous first-principles study<sup>30</sup> found that oxygen vacancies can greatly reduce the TMR and produces a resonant tunneling at a high bias of 1 V. We consider three different contents vacancy (0%, 0.5%, and 1%) using the coherent-potential approximation.<sup>31</sup> The rest of the structure is the same as before.<sup>4,27</sup> Calculations with less vacancies were not carried out because the extra peaks in the spectrum would diminish so much that it looks very similar to that of pure Fe/MgO/Fe structure.

The calculation for three types of junctions, symmetric Fe/MgO/Fe, asymmetric Fe/MgO/vacancy/Fe (0.5% and 1% vacancy), and Fe/FeO/MgO/Fe are shown in Fig. 3. For each calculation, the transmission probability is integrated over 8256  $\mathbf{k}$  points in the irreducible two-dimensional Brillouin zone. The total conductance including both majority and minority spins is plotted. For ideal Fe/MgO/Fe structure, there is one main peak at zero bias and two shoulders at about  $\pm 0.27$  V. For Fe/MgO/vacancy/Fe, in addition to the features similar to ideal Fe/MgO/Fe structure, there is also a strong peak at about +0.04 V and a shoulder at about +0.17 V. The peak positions are the same for different vacancy but the intensity increases with increasing vacancy content. For Fe/FeO/MgO/Fe, one strong peak appears in the negative bias at about -0.11 V. As a check of Eq. (2) we also plot for Fe/FeO/MgO/Fe the derivative of the  $I$ - $V$  curve<sup>28</sup> from the fully self-consistent nonequilibrium Green's function (NEGF) method in Fig. 3(b). The major peak near -0.11 V is in agreement for both calculations. The overall difference in the background arises from the omission of  $V\partial G/\partial V$  in Eq. (2), which moves the peak positions slightly toward lower biases, in addition to a change in the background. The minor peaks at 0.05 and 0.32 V are due to nonself-consistent interface resonance states which are removed by the NEGF self-consistent calculation and are not seen experimentally. The calculated spectra for the AP con-

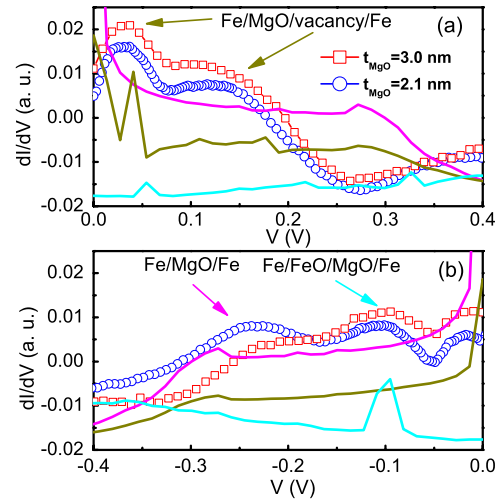


FIG. 4. (Color online)  $dI/dV$  for the P configuration for two junctions with  $t_{\text{MgO}}=2.1$  nm (open circles) and 3.0 nm (open squares) compared to calculations (solid curves) (a) positive bias and (b) negative bias. The major peaks for each curve are indicated by arrows.

figuration show no major peaks, in good agreement with experiment. For the symmetric Fe/vacancy/MgO/vacancy/Fe with 0.5% vacancy (not shown here), both the positive and the negative bias sides of the spectrum are essentially the same as the positive bias part of the asymmetric Fe/MgO/vacancy/Fe spectrum.

In Fig. 4 we compare the calculated  $G(E_F, V)$  with the measured  $dI/dV$  for the P configuration for two junctions with  $t_{\text{MgO}}=2.1$  and 3.0 nm shown by open circles and open squares, respectively. To facilitate the comparison, we plot the positive and negative biases separately in panels (a) and (b). A fourth-order polynomial background is removed from the experimental data to accentuate the peaks. Each calculated spectrum is also shifted by a constant in order to be plotted in the same range as the experimental data. The asymmetric structure of Fe/MgO/vacancy/Fe with 1% vacancy was used in Fig. 4. The solid lines in Fig. 4 from top to bottom are calculations for Fe/MgO/Fe, Fe/MgO/vacancy/Fe, and Fe/FeO/MgO/Fe structure, respectively. For the positive bias in Fig. 4(a), where the electrons are injected from the top electrode, an experimental peak at 0.026 V and a shoulder at 0.13 V are matched well with the calculated spectrum for the Fe/MgO/vacancy/Fe structure. For the negative bias in Fig. 4(b), where the electrons are injected from the bottom electrode, there are a peak at -0.11 V and a shoulder at around -0.24 V in the experimental spectrum. The former matches with the calculated peak for the Fe/FeO/MgO/Fe structure while the latter matches with the shoulder for the ideal Fe/MgO/Fe structure. It is reasonable to conclude that for the positive bias voltage, the main features in  $dI/dV$  are due to the Fe/MgO/vacancy/Fe structure and that for the negative bias voltage, the main features in  $dI/dV$  are due to the Fe/MgO/Fe and Fe/FeO/MgO/Fe structures.

There have been theoretical suggestions together with experimental support that the interface between the bottom electrode and the MgO layer likely has FeO,<sup>23,26,27</sup> and that the interface between the MgO layer and the top electrode

has dislocations and vacancies.<sup>7,32</sup> The results here present direct evidence of the existence of a mixture of Fe/MgO and Fe/FeO/MgO at the bottom interface, and the presence of oxygen vacancies at the top interface. Our measurement also suggests that only the interface on the side of the electrons injecting electrode determines the spin-dependent tunneling spectrum. This is consistent with the presence of diffusive scattering inside the MgO barrier layer. The previous estimate of the scattering length inside MgO barrier is about 2 nm.<sup>33</sup>

In summary, by carefully comparing the measured dynamic conductance of epitaxial Fe/MgO/Fe MTJs with first-principles calculation, the peaks in IET spectra can be related to the interface structure, where the bottom interface is a mixture of Fe/MgO and Fe/FeO/MgO, and the top interface contains some oxygen vacancies. Further refinement of both experiment and theory may allow spin-dependent tunneling spectroscopy to determine interface structures quantitatively.

For example, the difference in the relative heights of the two measured peaks for two samples in Fig. 4(b) might indicate different amount of FeO at the bottom interface in two samples, which was further proved by the MTJ samples with MgO barrier grown at 200 °C (not shown here) compared to room temperature used for this study.

This work was supported by the National Basic Research Program of China (MOST under Grants No. 2009CB929203 and No. 2006CB932200) and Chinese National Natural Science Foundation (NSFC under Grants No. 50972163 and No. 50721001). S.G. Wang is grateful to the Engineering and Physical Sciences Research Council (EPSRC) of U.K. for financial support. Portion of the research was conducted at the CNMS of ORNL, operated by UT-Battelle for Office of User Facilities, Basic Energy Sciences, U.S. Department of Energy.

\*Corresponding authors.

†sgwang@aphy.iphy.ac.cn

‡zhangx@ornl.gov

- <sup>1</sup>M. Julliere, *Phys. Lett. A* **54**, 225 (1975).
- <sup>2</sup>T. Miyazaki and N. Tezuka, *J. Magn. Magn. Mater.* **139**, L231 (1995).
- <sup>3</sup>J. S. Moodera, L. R. Kinder, T. M. Wong, and R. Meservey, *Phys. Rev. Lett.* **74**, 3273 (1995).
- <sup>4</sup>W. H. Butler, X.-G. Zhang, T. C. Schulthess, and J. M. MacLaren, *Phys. Rev. B* **63**, 054416 (2001).
- <sup>5</sup>J. Mathon and A. Umerski, *Phys. Rev. B* **63**, 220403(R) (2001).
- <sup>6</sup>S. S. Parkin, C. Kaiser, A. Panchula, P. M. Rice, B. Hughes, M. Samant, and S. H. Yang, *Nature Mater.* **3**, 862 (2004).
- <sup>7</sup>S. Yuasa, T. Nagahama, A. Fukushima, Y. Suzuki, and K. Ando, *Nature Mater.* **3**, 868 (2004).
- <sup>8</sup>C. Tiusan, J. Faure-Vincent, C. Bellouard, M. Hehn, E. Jouguet, and A. Schuhl, *Phys. Rev. Lett.* **93**, 106602 (2004).
- <sup>9</sup>S. G. Wang, R. C. C. Ward, G. X. Du, X. F. Han, C. Wang, and A. Kohn, *Phys. Rev. B* **78**, 180411(R) (2008).
- <sup>10</sup>S. Ikeda, J. Hayakawa, Y. Ashizawa, Y. M. Lee, K. Miura, H. Hasegawa, M. Tsunoda, F. Matsukura, and H. Ohno, *Appl. Phys. Lett.* **93**, 082508 (2008).
- <sup>11</sup>T. Nozaki, N. Tezuka, and K. Inomata, *Phys. Rev. Lett.* **96**, 027208 (2006).
- <sup>12</sup>X. F. Han, J. Murai, Y. Ando, H. Kubota, and T. Miyazaki, *Appl. Phys. Lett.* **78**, 2533 (2001).
- <sup>13</sup>Y. Ando, T. Miyakoshi, M. Oogane, T. Miyazaki, H. Kubota, K. Ando, and S. Yuasa, *Appl. Phys. Lett.* **87**, 142502 (2005).
- <sup>14</sup>G. X. Miao, K. B. Chetry, A. Gupta, W. H. Bulter, K. Tsunekawa, D. Djayaprawira, and G. Xiao, *J. Appl. Phys.* **99**, 08T305 (2006).
- <sup>15</sup>S. Nishioka, R. Matsumoto, H. Tomita, T. Nozaki, Y. Suzuki, H. Itoh, and S. Yuasa, *Appl. Phys. Lett.* **93**, 122511 (2008).
- <sup>16</sup>K. Ono, T. Daibou, S. J. Ahn, Y. Sakuraba, T. Miyakoshi, T. Morita, Y. Kikuchi, M. Oogane, Y. Ando, and T. Miyazaki, *J. Appl. Phys.* **99**, 08A905 (2006).
- <sup>17</sup>I. Rungger, O. Mryasov, and S. Sanvito, *Phys. Rev. B* **79**, 094414 (2009).
- <sup>18</sup>P.-J. Zermatten, G. Gaudin, G. Maris, M. Miron, A. Schuhl, C. Tiusan, F. Greullet, and M. Hehn, *Phys. Rev. B* **78**, 033301 (2008).
- <sup>19</sup>R. Guerrero, D. Herranz, F. G. Alieva, F. Greullet, C. Tiusan, M. Hehn, and F. Montaigne, *Appl. Phys. Lett.* **91**, 132504 (2007).
- <sup>20</sup>S. Zhang, P. M. Levy, A. C. Marley, and S. S. P. Parkin, *Phys. Rev. Lett.* **79**, 3744 (1997).
- <sup>21</sup>P. LeClair, J. T. Kohlhepp, H. J. M. Swagten, and W. J. M. de Jonge, *Phys. Rev. Lett.* **86**, 1066 (2001).
- <sup>22</sup>C. Wang, S. G. Wang, A. Kohn, R. C. C. Ward, and A. K. Petford-Long, *IEEE Trans. Magn.* **43**, 2779 (2007).
- <sup>23</sup>S. G. Wang, G. Han, G. H. Yu, Y. Jiang, C. Wang, A. Kohn, and R. C. C. Ward, *J. Magn. Magn. Mater.* **310**, 1935 (2007).
- <sup>24</sup>S. G. Wang, A. Kohn, C. Wang, A. K. Petford-Long, S. Lee, R. Fan, J. P. Goff, L. J. Singh, Z. H. Barber, and R. C. C. Ward, *J. Phys. D* **42**, 225001 (2009).
- <sup>25</sup>Q. L. Ma, S. G. Wang, J. Zhang, Y. Wang, R. C. C. Ward, C. Wang, A. Kohn, X.-G. Zhang, and X. F. Han, *Appl. Phys. Lett.* **95**, 052506 (2009).
- <sup>26</sup>H. L. Meyerheim, R. Popescu, J. Kirschner, N. Jedrecy, M. Sauvage-Simkin, B. Heinrich, and R. Pinchaux, *Phys. Rev. Lett.* **87**, 076102 (2001).
- <sup>27</sup>X.-G. Zhang, W. H. Butler, and A. Bandyopadhyay, *Phys. Rev. B* **68**, 092402 (2003).
- <sup>28</sup>C. Zhang, X.-G. Zhang, P. S. Krstić, H.-P. Cheng, W. H. Butler, and J. M. MacLaren, *Phys. Rev. B* **69**, 134406 (2004).
- <sup>29</sup>J. M. MacLaren, X.-G. Zhang, W. H. Butler, and X. Wang, *Phys. Rev. B* **59**, 5470 (1999).
- <sup>30</sup>J. P. Velev, K. D. Belashchenko, S. S. Jaswal, and E. Y. Tsymlal, *Appl. Phys. Lett.* **90**, 072502 (2007).
- <sup>31</sup>J. S. Faulkner and G. M. Stocks, *Phys. Rev. B* **21**, 3222 (1980).
- <sup>32</sup>J. Ozeki, H. Itoh, and J. Inoue, *J. Magn. Magn. Mater.* **310**, e644 (2007).
- <sup>33</sup>X.-G. Zhang, Y. Wang, and X. F. Han, *Phys. Rev. B* **77**, 144431 (2008).